THE JOURNAL OF PHYSICAL CHEMISTRY B

Article

Cite This: J. Phys. Chem. B 2019, 123, 2756−2769

pubs.acs.org/JPCB

Structure Relaxation Approximation (SRA) for Elucidation of Protein Structures from Ion Mobility Measurements

Published as part of The Journal of Physical Chemistry virtual special issue "Young Scientists".

Christian Bleiholder* and Fanny C. Liu

Department of Chemistry and Biochemistry, Florida State University, Tallahassee, Florida 32306, United States

Supporting Information

ABSTRACT: Ion mobility spectrometry−mass spectrometry methods offer the potential to correlate protein tertiary and quaternary structures to variations in their amino acid sequences and post-translational modifications. Because ion mobility spectrometry measures cross sections of ions in the gas phase, however, the structure of protein systems detected by ion mobility spectrometry will generally differ from their native solution structures. While it is now established that ion mobility spectrometry does not typically detect equilibrium gas-phase structures of protein systems, what remains disputed is which aspects, if any, of the detected ions resemble the native state present in solution. Here, we develop the structure relaxation approximation (SRA) method to predict charge-state specific ion mobility spectra from an ensemble of solution structures. This allows us to predict the "global" trends observed in the experiments for various experimental conditions and charge states, thereby enabling detailed structure elucidation. The SRA predicts (RMSD to experiment ∼4%) that even the small protein ubiquitin largely retains its native inter-residue contacts with an intact hydrophobic core when studied by "soft" ion mobility measurements. Because collisional activation is increasingly inefficient with increasing numbers of internal degrees of freedom, the SRA suggests that it is all the more likely that ion mobility spectrometry retains essentially the native state for protein systems larger than ubiquitin.

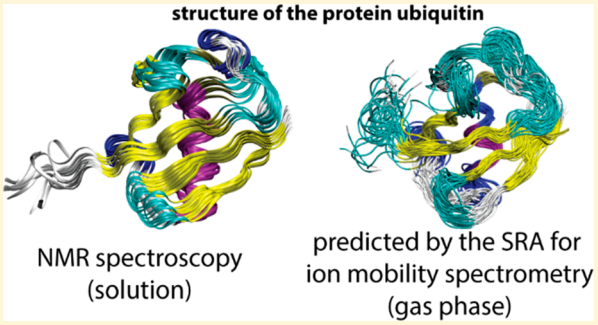

INTRODUCTION

The function of proteins and their assemblies is directly related to the structures they adopt and to the motions by which they interconvert.[1,2] This structure−function relationship takes on increased complexity because differentially modified variants of the same protein (proteoforms) frequently coexist.[3] While proteoforms originate from the same gene, they differ in their amino acid sequences and/or post-translational modifications and often exhibit divergent biological activity.[4] Hence, it is imperative to identify how individual proteoforms differ in their tertiary and quaternary structures.

Ion mobility spectrometry−mass spectrometry methods[5,6] offer the potential to address this question. Tandem-mass spectrometry can reveal (partial) amino acid sequences of proteoforms[7,8] as well as the identity and location of post-translational modifications.[9,10] Coupling with ion mobility spectrometry allows the analyst to characterize their structures by momentum transfer cross sections.[6,11−14] Collision-induced unfolding ion mobility experiments[11,15,16] measure how ion cross sections change as the protein ions unfold in the gas phase due to vibrational activation. Such measurements provide additional information about the protein structure by characterizing energy barriers associated with the unfolding process.[15,17] Used in combination, these ion mobility spectrometry-mass spectrometry approaches offer the potential to correlate protein tertiary and quaternary structures to variations in their amino acid sequences and post-translational modifications.[18] Particularly promising appear tandem-ion mobility methods[19,20] that could perform these measurements for a specific, ion mobility-selected conformation of a proteoform.

Despite these promises, however, it remains unclear how useful ion mobility data are to investigate biological problems. Ion mobility spectrometry determines the cross section of an ion from measuring the velocity it acquires when traversing a gas-filled chamber under the influence of an electric field.[21−23] Ions that differ in size and shape acquire different velocities because they experience different resistances as they migrate and collide with the gas particles. Ion mobility spectrometry thus measures cross sections of desolvated protein ions in the gas phase. The gas phase, however, is a hydrophobic environment whereas the native state of a protein is determined in a complex environment, but in particular through interactions with hydrophilic water molecules or ions.[24,25] Consequently, the equilibrium structure of a protein in the gas phase may bear little resemblance to the

Received: December 7, 2018
Revised: March 6, 2019
Published: March 13, 2019

DOI: 10.1021/acs.jpcb.8b11818
J. Phys. Chem. B 2019, 123, 2756−2769

natively folded protein structure, potentially by turning "inside-out"[26,27] or by unfolding into extended (α-helical) structures.[28−30] This view suggests that ion mobility measurements may not reflect the behavior of the protein's native state, disconnecting the measurement from the biological problem of interest.

Thus, the key question is, How closely do the structures of the desolvated protein ions detected in an ion mobility measurement correspond to the biologically active native state?

There is clear-cut experimental evidence that ion mobility measurements do not detect gas-phase equilibrium structures of protein systems when conducted under "soft" operating conditions where ions do not experience energizing collisions with gas particles.[31] Even for small proteins like cytochrome C or ubiquitin, time-resolved ion mobility measurements suggest gas-phase isomerization times on the order of up to several seconds for low charge states.[32,33] Solvent conditions were also found to strongly influence ion mobility spectra.[31,34] Furthermore, charge-reduction[35,36] and collisional-unfolding[37] experiments exhibit a marked "hysteresis" in the sense that protein ions detected from native solution conditions are significantly more compact than their isomers produced from refolding in the gas phase. These experiments, to mention just a few, demonstrate that protein ions are metastable and do not typically reach their equilibrium gas-phase structure within the time scale of "soft" ion mobility experiments.[31] Hence, protein systems are detected as their structures are in the process of transitioning from the solution into the gas-phase equilibrium structure and the principle of ergodicity does not apply (Figure 1A). These considerations suggest that ion mobility spectrometry provides biologically relevant information for those aspects of the native state that are retained within the time scale of the measurement.

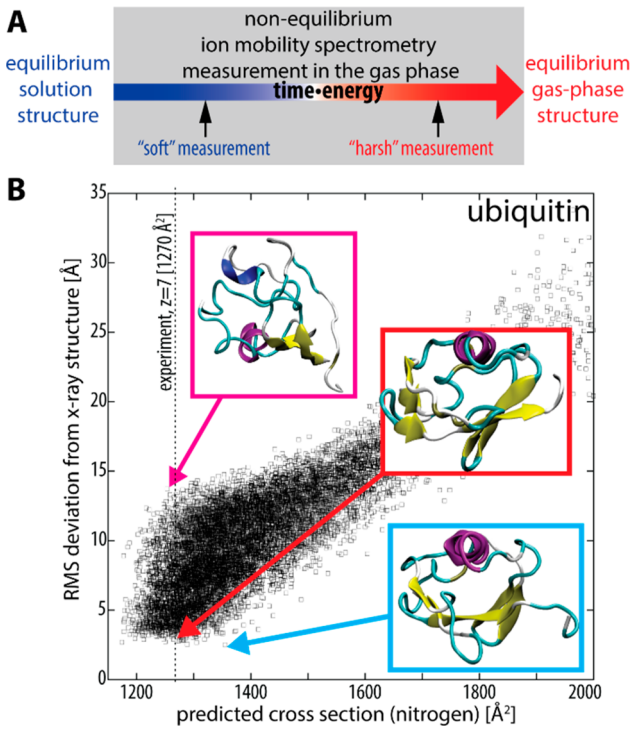

Figure 1. (A) Structures of protein ions detected by "soft" ion mobility spectrometry are in the process of transitioning from the solution to the gas-phase equilibrium structures. These are thus nonergodic experiments. (B) Different protein structures may have the same cross section. Therefore, similarity in cross sections is a *necessary but not a sufficient criterion* for similarity in structures.

What these experiments do not reveal, however, is what aspects of the native state, if any, are retained in ion mobility measurements. To address this question, one has to interpret the ion mobility data in terms of the protein structure. The accepted approach is to calculate cross sections for candidate model structures and then assign a structure that matches the experimental cross section. This approach of matching singular cross section values was applied with great success to carbon[38] and silicon[39] clusters, and small gas-phase systems[40,41] that adopt a limited set of conformations. Nonetheless, even for protein systems, it is frequently observed that cross sections predicted for their NMR or X-ray structures agree closely with cross sections measured for low protein charge states.[31,42,43] In fact, such consistencies between ion mobility data and X-ray and NMR structures embody the main argument to support that ion mobility measurements detect the (native) solution structure even for the small protein ubiquitin.[31] But is consistency in cross section a sufficient criterion for similarity in structures?

The answer is clearly that it is not, because different protein structures may have the same cross section. Let us bear in mind that a cross section is a two-dimensional "effective" area of an ion[44] and that a protein with n residues can adopt on the order of 3^{2n} backbone conformations.[45] Because many of these (three-dimensional) conformations have the same (two-dimensional) cross section, it is possible to assign a plethora of different structures to a measured cross section value, even for proteins as small as ubiquitin (Figure 1B). Furthermore, because side chain orientations considerably influence the cross section of a protein structure, it is also possible to assign the "native" backbone conformation to a wide range of measured cross sections—in the case of ubiquitin, from ∼1180 to ∼1350 Å^2 (Figure 1B). Indeed, if similarity in cross sections were a sufficient criterion to infer similarity in structures, then it would follow from charge-reduction experiments[35] that ubiquitin charge states 3+ and 4+ refold into their native solution structures in the absence of solvent.

Considering these ambiguities of interpreting cross sections, can ion mobility actually be used to infer structural details of ions? Experimental evidence on carbon clusters[38,46] and peptide assemblies[12,47] shows that detailed structural assignments from ion mobility data are indeed possible. For example, we concluded from ion mobility data alone that the hexapeptide VEALYL forms β-sheet assemblies starting from the dimer,[12] which was later confirmed by ion spectroscopy.[48]

These ion mobility studies, however, refrain from interpreting individual cross sections and also refrain from selecting model structures by matching computed and experimental cross sections. By contrast, these studies assign structures from *comparing the overall trends that emerge from the entirety of the experimental cross sections* (i.e., charge states, assembly states, etc.) to the *overall trends predicted for structural families*. This suggests that globally comparing experimental and predicted ion mobility spectra could represent a general approach to assigning detailed structures to ions detected by ion mobility spectrometry.

Here, we describe the structure relaxation approximation (SRA) method. The SRA allows us to apply this principle of globally interpreting ion mobility spectra for a system of interest using a molecular dynamics-based approach. The central aspect of the SRA is to account for lack of ergodicity in the experiment, thereby allowing us to predict charge-state specific ion mobility

DOI: 10.1021/acs.jpcb.8b11818
J. Phys. Chem. B 2019, 123, 2756−2769

spectra from an ensemble of solution structures. The more charge states and experimental conditions are probed by experiment and theory, the greater the confidence of the structural interpretation because chance agreement for all conditions becomes increasingly unlikely. We subsequently apply the SRA method to probe how closely, and in which aspects, ions of the protein ubiquitin detected by "soft" ion mobility measurements resemble the native state. The SRA predicts that even the small protein ubiquitin retains essentially the same residue−residue contacts as the native structure determined by X-ray crystallography when measured by "soft" ion mobility methods.

METHODS

A full description of the methods is given in the Supporting Information. Briefly, ion mobility measurements were performed on a recently developed tandem-TIMS-Qq-TOF instrument (Figure S1, Supporting Information) described in detail elsewhere[20] with nitrogen buffer gas (Peak Scientific nitrogen generator, NM32-LA-MS-230 V). Bovine ubiquitin (Sigma-Aldrich, St. Louis, MO) was diluted to 10 μM in LC/MS grade water (Fisher Scientific, Waltham, MA) and water/methanol (Acros Organics, Pittsburgh, PA), both with 1% acetic acid (pH ∼ 3, LC/MS grade, Fisher Scientific). Note that ubiquitin is stable in aqueous solutions at pH above 2 ($T_m \approx 55$ °C).[49] Samples were directly infused into the electrospray ionization source (positive mode) by a gastight syringe (Hamilton, Franklin, MA) at flow rates of 80−180 μL/h. Instrument settings were taken from previous studies.[20,50] We emphasize that these settings reproduce "soft" drift-tube spectra of ubiquitin;[51,52] as discussed,[47,50] this means that our work does not suffer from ion heating. Ions produced from electrospray are deflected into the first TIMS device (TIMS-1). Ions traverse an entrance funnel, are mobility-separated in the first TIMS analyzer tunnel, and exit TIMS-1 through an ion funnel. Subsequently, they traverse two apertures and enter the second TIMS analyzer (TIMS-2) through deflector-2. As reported,[20] by timing a blocking electric potential between aperture-1 and aperture-2, we prevent ions from entering TIMS-2, thereby mobility-selecting ions. By timing an activating potential between aperture-2 and deflector-2, we can vibrationally activate the selected ion by energetic ion−neutral collisions. The selected ions traverse an ion funnel, are mobility-separated in the mobility analyzer of TIMS-2, and exit TIMS-2 through another ion funnel. Entrance and exit pressures were set to 3.2 and 1.6 mbar (TIMS-1) and 0.9 and 0.3 mbar (TIMS-2). Cross sections were calibrated as described[53−56] using perfluorated phosphazenes contained in Agilent ESI tuning mix (m/z 622, 922, 1522) with reported[56,57] reduced ion mobilities (1.016, 0.841, 0.642 cm^2/(V s)).

Initial structures were taken from the protein data bank (PDB) and from a previous study (A-state; acidic methanol/water).[58] Explicit-solvent molecular dynamics calculations were carried out with GROMACS[59] in conjunction with the amber ff03 force field[60] and the TIP3P[61] and meoh[62] solvent models for water and methanol, respectively. More details are found in section S2.3.2 (Supporting Information). Gas-phase molecular dynamics simulations were carried out with GROMACS in conjunction with the OPLS-AA force field,[63,64] because this force field was rigorously fitted to *ab initio* potential energy surfaces and accurately reproduces *ab initio* conformational energies of tetrapeptides.[64,65] Theoretical cross sections were computed by the projection superposition approximation (PSA) method for helium[66−69] and nitrogen[51] gases. Solvent accessible surface areas were calculated by the POPS algorithm.[70] The MOPAC[71] package was used for all electronic structure calculations.

RESULTS AND DISCUSSION

The mass spectrum recorded on our tandem-TIMS-Qq-TOF instrument for ubiquitin electrosprayed from an aqueous solution shows mainly charge states 5+ through 8+ (Figure 2A). This charge-state distribution is typical for solution

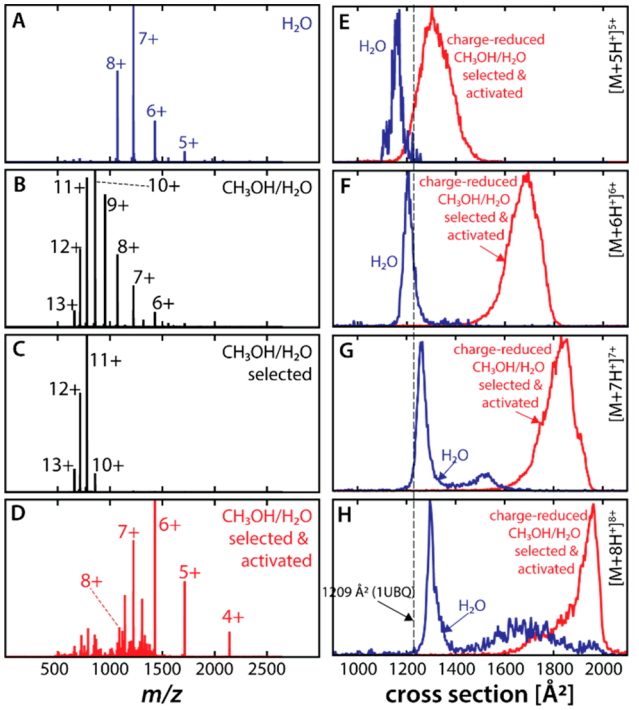

Figure 2. (A)−(D) Positive ion mass spectra recorded for ubiquitin under different conditions: (A) aqueous solution with 1% acetic acid; (B) methanol/water with 1% acetic acid without mobility-selection; (C) selection of ions between TIMS-1 and TIMS-2 with reduced mobility ≈0.91−0.98 cm^2/(V s); (D) selection and activation of ions by 250 V between TIMS-1 and TIMS-2, which results in backbone fragment ions and charge-reduced $[M + zH]^{z+}$. (E)−(H) Ion mobility spectra for $[M + zH]^{z+}$ species with $z = 4$−8 observed in (A), blue trace, and observed in (D), red trace.

conditions in which the native state of ubiquitin is stable.[31,34] The native state of ubiquitin unfolds into the partially folded A-state in acidic methanol/water.[72] This conformational change is noticeable in the mass spectrum by dominance of charge states 9+ to 11+ (Figure 2B). Next, we generate ions from acidic methanol/water but only allow ions with reduced mobilities between 0.91 and 0.98 cm^2/(V s) to pass through the interface between TIMS-1 and TIMS-2 (Figure 2C). As described in detail elsewhere,[20] we achieve this mobility selection by timing a blocking electric potential between aperture-1 and aperture-2 (Figure S1, Supporting Information). Figures 2C and S2 (Supporting Information) show that this effectively removes ubiquitin charge states lower than +10 from the spectrum. Next, we collisionally activate the selected ions by placing a voltage of 250 V between aperture-2 and deflector-2 (Figure 2D). Consistent with our previous report,[20] b- and y-type fragment ions are abundantly formed. In addition to these backbone

DOI: 10.1021/acs.jpcb.8b11818
J. Phys. Chem. B 2019, 123, 2756−2769

cleavages, however, Figure 2D shows abundant formation of m/z 2141, 1713, 1428, 1224, 1071.

A closer inspection of the isotopic patterns for m/z 2141, 1713, 1428, 1224, 1071 shows that these ions are protonated ubiquitin species $[M + zH]^{z+}$ with z = 4−8 (see Figure S2, Supporting Information). Note that the isotopic patterns are inconsistent with radical species formed by addition of electrons such as those described for electron-capture[28] or electron transfer without dissociation.[36] Because these charge-reduced species are only present after collisional activation (see Figure 2C,D and S2, Supporting Information), they must be formed by removing protons from the selected ubiquitin ions as these are collisionally activated between aperture-2 and deflector-2.

While the mechanistic details of how protons are removed from the vibrationally excited higher charges states are part of ongoing work, what is clear from the data is the following: the $[M + zH]^{z+}$ ions in Figure 2D are protonated ubiquitin species with the same molecular formula as the $[M + zH]^{z+}$ ions detected from an aqueous ubiquitin solution (Figure 2A). Consequently, for the same charge state, the structures adopted by $[M + zH]^{z+}$ in Figure 2A,D correspond to distinct isomers on the same Born−Oppenheimer potential energy surface.

Parts E−H of Figure 2 compare the ion mobility spectra of charge states 5+ to 8+ observed in Figure 2A (aqueous solution) to those observed in Figure 2D (proton transfer in the gas phase from ions produced from an acidic methanol/water solution). Consistent with drift tube measurements in helium[31,34] and nitrogen,[51] the spectra recorded from the aqueous ubiquitin solution show one dominant peak. The cross sections of these peaks (1160−1299 Å^2, see Table S1 in the Supporting Information) are consistent with the cross section expected for the ubiquitin X-ray structure[51] and with measurements conducted on drift tubes.[47,51,52] Further, and also in line with previous reports,[35,36] the charged-reduced species (1317−1977 Å^2) are significantly smaller than their precursor ions before proton transfer (∼2200−2600 Å^2; see Table S1 in the Supporting Information). This compaction indicates that the charge-reduced ubiquitin ions refold in the gas phase after proton transfer. Nevertheless, these gas phase-folded ubiquitin species are larger than their isomers detected from an aqueous solution (see Figure 2E−H). This apparent "hysteresis" means that the ubiquitin ions detected as charge states 5+ to 8+ from an aqueous solution have not been able to isomerize into their equilibrium gas-phase structures during the course of the ion mobility measurement. As discussed in the Introduction, the same conclusion follows from other reports.[31−37]

Clearly, the main features of $[M + 5H]^{5+}$ to $[M + 8H]^{8+}$ produced from aqueous conditions are consistent with the ubiquitin X-ray structure. But may we infer from this consistency that the structures of these ions correspond to the native state? Consider the cross sections of the charge-reduced species $[M + 4H]^{4+}$ and $[M + 5H]^{5+}$ (1182 Å^2 and 1317 Å^2; see Figure 2 and Table S1, Supporting Information). Their cross sections are also consistent with the nitrogen cross section calculated[51] for the X-ray structure (1209 Å^2). Note also that helium cross sections reported[35] for ubiquitin $[M + 3H]^{3+}$ and $[M + 4H]^{4+}$ produced by proton-abstraction from $[M + 13H]^{13+}$ agree well with the cross section expected for the native state.[51] Assuming that consistency in cross section were a *necessary and sufficient criterion* for similarity in structures, these observations would imply that ubiquitin ions refold into native(-like) structures in the absence of solvent. Obviously, this is highly unlikely because folding of the charge-reduced species occurs in the hydrophobic gas phase, whereas folding of native protein structures is governed through interactions with water molecules.[25] These discussions highlight that a consistency in cross section is a *necessary but not a sufficient criterion* for structural similarity. Hence, establishing consistencies between measured cross sections and cross sections predicted for individual model structures cannot represent an appropriate approach to confidently elucidate structures from ion mobility data, at least not for structurally complex species.

The relevant questions are thus: (1) What are the structures of the $[M + 5H]^{5+}$ to $[M + 8H]^{8+}$ ubiquitin ions produced from aqueous conditions? (2) In which aspects do the structures of these ions resemble the native ubiquitin structure as determined by NMR or X-ray spectroscopy? (3) In which aspects do the structures of these ions differ from their gas-phase isomers (produced from refolding in the gas phase after proton-abstraction)?

Structure Relaxation Approximation (SRA). To address these three questions above, we developed the structure relaxation approximation (SRA) method to allow us to globally interpret ion mobility spectra for a system of interest using a molecular dynamics-based approach. The central aspect of the SRA is to account for lack of ergodicity in order to *predict* ion mobility spectra by taking as input (a) an ensemble of solution structures and (b) the ion charge state. This means that for experiments conducted under the same conditions, predictions are fully defined by the charge state of the detected ions. For experiments conducted under equivalent operating conditions but from different solvents, predictions may differ only in the ensemble of initial solution structures. Hence, the more charge states and solution conditions are probed, the greater the confidence of the structural interpretation because chance agreement between experiment and prediction for all spectra becomes increasingly unlikely. We implemented the SRA as a configurable and automatized software program (for details see section S2, Supporting Information).

The SRA takes as input an ensemble of solution structures (typically ∼2000 structures; for example from molecular dynamics simulations) and assumes an "instantaneous desolvation" in line with reports that structural changes during the desolvation process of proteins involve mainly the reorientation of side chains but not the protein backbone.[73−75] After solvent removal, three steps are sequentially applied to each input structure:

(1) The first step is to add protons to (or remove protons from) the structure so that its formal charge matches the charge state z of the ion $[M + zH]^{z+}$ detected in the experiment. This step is required because the charge state is known to significantly influence the ion mobility spectrum via structural dynamics of the ions.[32,34,76] Our logic in this step is that amino acid residues that are more exposed to the solvent are more likely to be charged. This is based on prior work, which showed that the charge states of protein ions observed in mass spectrometry are highly correlated to their solvent accessible surface area.[77] Hence, we determine the formal charge of each amino acid residue and then add (or remove) protons from chargeable residues (Glu, Asp, His, Arg, Lys) with the largest solvent accessible surface areas. To this end, we calculate atomic partial charges and add a proton in proximity to the most negatively charged heteroatom of the selected residue (or remove its most positively

DOI: 10.1021/acs.jpcb.8b11818
J. Phys. Chem. B 2019, 123, 2756−2769

charged proton). We then optimize the hydrogen positions using Stewart's local SCF method[78] and recalculate the Lewis structure to assert a chemically correct protein structure. Chemically incorrect structures are obtained in about 10−15% of the cases and discarded from further analysis. This approach broadly samples protomers; see Figure S16 (Supporting Information) for protomers sampled for charge states 6+ to 8+ from aqueous solution. Our approach thus appears more appropriate than algorithms that minimize an energy function[79] during the gas-phase simulation, which tend to converge to a "global minimum protomer" that subsequently dominates the molecular dynamics simulations.[74]

(2) The second step is to relax the structure of the protein ion *in direction toward, but not into*, its gas-phase equilibrium structure. This step is required because "soft" ion mobility measurements[47] detect kinetically trapped (metastable) protein systems as their structures are in the process of transitioning from the solution into the gas-phase equilibrium structure. This means that ion mobility spectrometry is inherently a nonequilibrium method in these measurements and the principle of ergodicity does not apply to these experiments. Hence, methods that are devised to sample large regions of phase space by efficiently crossing high-energy barriers, such as replica-exchange molecular dynamics[80] or metadynamics,[81,82] are not appropriate to simulate the gas-phase relaxation process of protein systems in ion mobility measurements recorded under "soft" conditions. To account for lack of ergodicity in the experiment, we thus perform short (typically <5 ns) molecular dynamics simulations of the charged protein ion in the gas phase (see below and Figure S4, Supporting Information, for details). Depending on the energy and time length of these simulations, this approach allows the protein ions to overcome some of the energy barriers and change toward to, but not into, the equilibrium gas-phase structure.

(3) Subsequently, we account for structural dynamics of the ions during the ion mobility measurement. To this end, we propagate trajectories at 300 K and average the cross section over the sampled snapshots (Figure S4, Supporting Information). In our experience, calculating cross sections for ∼10% of the snapshots yields appropriate average cross sections (see Figure S5, Supporting Information). Because an average cross section is calculated for each of the ∼2000 initial (solution) structures from averaging ∼20 individual cross sections, each predicted spectrum shown below requires on the order of 30 000−40 000 individual cross section calculations. We hence use our projection superposition approximation (PSA) method[51,66−69] for these cross section calculations, which yields accurate cross sections for both helium and nitrogen buffer gases at significantly lower computational efforts than other accurate methods.[39,83−85] Note that approaches that account for the ion shape through statistical fitting procedures[86,87] incorrectly imply that shape effects are independent of the charge state and/or geometry of the ion and result in errors of up to ∼10% (Figures S6 and S7, Supporting Information).

Finally, the ion mobility spectrum is then calculated as the sum of Gaussian distributions centered at each of the averaged cross sections and the standard deviation given by the experimental resolving power as described in section S2.3.6 (Supporting Information).

As expected from prior work,[76] a spectrum predicted by the SRA depends critically on the time length and energy of the gas-phase simulations performed in step 2. Figure S4 (Supporting Information) reveals the effect of different energies and time lengths of the gas-phase relaxation simulation on the predicted ion mobility spectrum of ubiquitin charge state $[M + 6H]^{6+}$. Short simulation time lengths and low simulation energies marginally affect the protein structure because only few energy barriers are overcome in the gas phase. As the ions are given more time and energy, however, they are increasingly able to adopt to the gas-phase environment by overcoming larger barriers and relaxing toward the gas-phase structure. This increased efficiency of the gas-phase relaxation process is noticeable in Figure S4 by the increased abundance of extended structures with sections between ∼1300 Å^2 and 1800 Å^2 as the length and energy of the simulation are increased. To accurately predict ion mobility spectra, we must therefore identify the time and energy that best reflects the effective ion temperature[21−23] in the experiments. We identify the combination of simulation time length and energy that best corresponds to the experiment by calculating the cross correlation and coherence between the experimental and predicted ion mobility spectra for $[M + 6H]^{6+}$ (T_{max} = 600 K; see Figure S4, Supporting Information, for details). Because the effective ion temperature does not significantly depend on the reduced ion mobility in the low-field limit,[21−23] prediction of other spectra measured under equivalent experimental conditions must now be made using this same gas-phase relaxation protocol.

Predicting Ion Mobility Spectra with the Structure Relaxation Approximation (SRA) Method. We apply the SRA to predict the experimental trends observed for different charge states, buffer gases, and initial conditions (such as aqueous or methanol/water solutions, charge reduction in the gas phase) of the protein ubiquitin.

Figure 3 compares ion mobility spectra predicted by the SRA to experimental data recorded for various charge states and solution conditions of ubiquitin observed in Figure 2. The SRA predictions started from snapshots taken during explicit-solvent molecular dynamics simulations and, for predictions of charge-reduced species, from structures predicted for $[M + 11H]^{11+}$ and $[M + 12H]^{12+}$ after gas-phase relaxation. We stress that all SRA predictions differ only in their input ensemble and/or their charge state; all other parameters are equal. Cross correlation shows a root-mean-square deviation (RMSD) between SRA and the experiment of ∼4.4% (nitrogen buffer gas) and that predicted and experimental spectra are strongly correlated (see section S2.3.7 and Figure S9, Supporting Information, for details). Figure S8 (Supporting Information) compares SRA predictions to previously reported[31,35] measurements carried out on drift tubes in helium buffer gas (RMSD = 3.7%, see Figure S9, Supporting Information).

When comparing experimental ion mobility data to those predicted by theory, it is critical to consider the accuracy of ion mobility theory. Due to space limitations, we limit ourselves to briefly discussing the "gold standard" trajectory method for helium buffer gas.[83] While trajectory methods correctly capture the physics of the collision process through propagating collision trajectories, for accuracy they rely on an intermolecular force

DOI: 10.1021/acs.jpcb.8b11818
J. Phys. Chem. B 2019, 123, 2756−2769

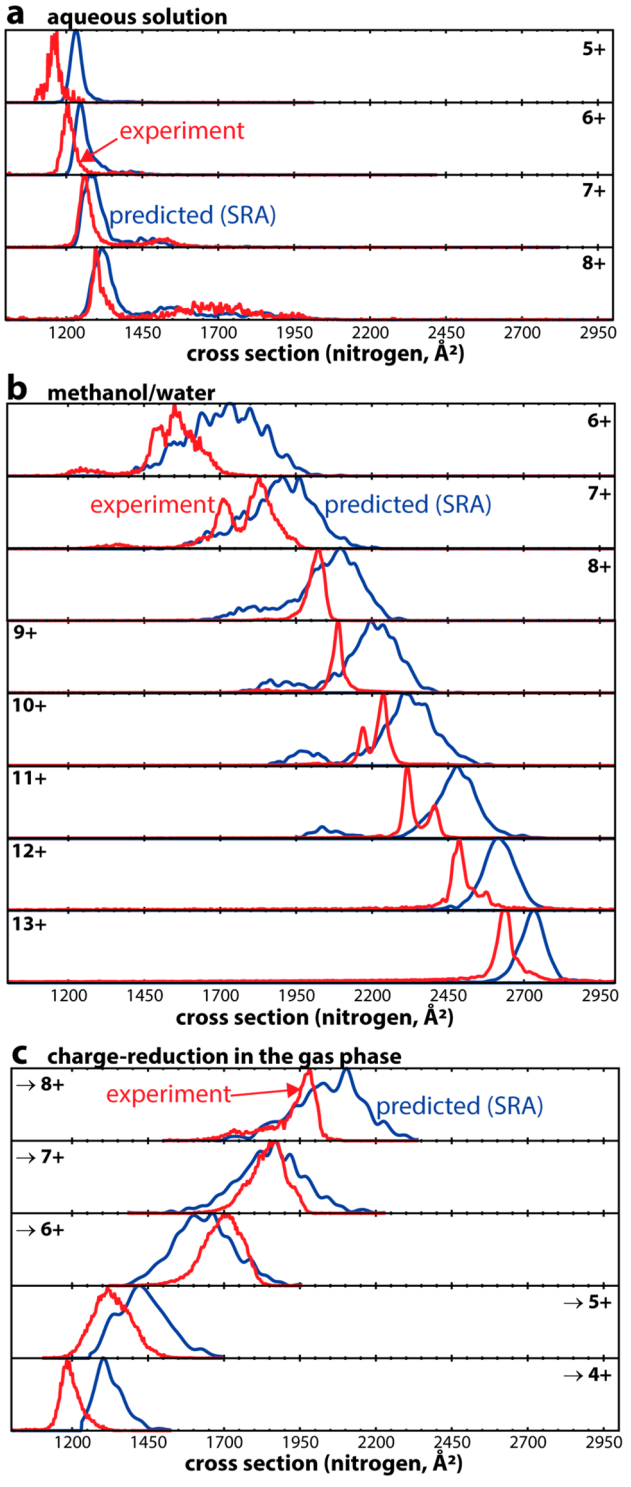

Figure 3. Comparison between experimental ion mobility spectra (red trace) and spectra predicted by the SRA (blue trace) for ubiquitin in nitrogen buffer gas for (A) aqueous solution and (B) methanol/water solution and for (C) charge reduction after mobility-selecting $[M + zH]^{z+}$ with $z > 9$ in the TIMS−TIMS interface. Experimental data are identical to those shown in Figure 2. SRA predictions for (A) and (B) started from structures observed during explicit-solvent molecular dynamics simulations and for (C) from structures predicted for $[M + 11H]^{11+}$ and $[M + 12H]^{12+}$ after gas-phase relaxation. Note that agreement between experiment and prediction (RMSD ∼ 5%) is within the errors of the methods.

field on which these trajectories are propagated. The only rigorous parametrization, however, was conducted for the element carbon in helium buffer gas, namely, by inverting temperature-dependent helium cross sections of C_{60}.[83] Furthermore, because oxygen and nitrogen atoms are treated as carbons, proteins are approximated to resemble carbon clusters. These approximations and others, discussed by us elsewhere,[66−69,88,89] result in errors of ∼5% even when the trajectory method is applied to systems as small as pentapeptides.[69] Hence, it follows that agreement between calculated and experimental cross sections of better than ∼5% is beyond the ability of the methods currently available.

The agreement between the spectra predicted by the SRA and the experimental spectra (RMSD 4.4% and 3.7%) is thus within the error of the methods. Further optimizations, or use of scaling factors, that increase agreement with the experiment would thus suggest a degree of accuracy that is inconsistent with the current limitations of ion mobility theory. Furthermore, predicted spectra tend to be slightly shifted to higher cross sections, which indicates a slight systematic error in the cross section calculations. These minor deviations from the experimental spectra are thus entirely expected from our previous reports.[66−69,88,89]

Figure 4 plots the cross sections of the main features observed in the measured and SRA spectra of ubiquitin as a function of the charge state for both helium and nitrogen gas. This global comparison demonstrates that our SRA method accurately predicts the trends observed in the experiments regardless of charge state, buffer gas, and initial (solution) condition. Most significant for the remainder of our discussion is the fact that the SRA quantitatively predicts the "hysteresis" of ubiquitin: ions produced from refolding in the gas phase are predicted to be similar in cross section to those produced from acidic methanol/water but significantly more extended than their isomers produced from aqueous conditions. Notice that our method truly *predicts* these trends for 34 spectra with varying charge states, solution conditions, and buffer gases. Hence, it is highly unlikely that the observed agreement between our predictions and the experiments is accidental, underscoring the validity of the SRA method.

Soft Ion Mobility Measurements Largely Retain the Native Structure of the Protein Ubiquitin. In the following, we thus discuss the structural predictions made by the SRA by analyzing the main peaks of the predicted spectra.

Does Ubiquitin Turn Inside-out after Solvent Evaporation? Ubiquitin is a small (8.6 kDa) protein that contains 11 acidic residues (five Asp and six Glu residues) and 12 basic residues (seven Lys, four Arg, and one His residues) in addition to the N and C termini.[90] These hydrophilic residues are exposed to the solvent in the ubiquitin native structure. By contrast, hydrophobic residues are found excluded from the solvent in a hydrophobic core. A hydrophobic core is common to protein systems because hydrophobic moieties do not favorably interact with the hydrophilic solvent water and "collapse" onto each other. In the gas phase, however, the situation is reversed. Here, the environment is hydrophobic and one might expect that a protein structure would turn "inside-out".[26,27]

To probe if ubiquitin turns inside-out in our ion mobility measurements, we extract the structures that compose the main features of the SRA spectra and calculate their mean hydrophobic and hydrophilic solvent accessible surface areas (Figure 5A). As reference, we also include the hydrophilic and hydrophobic surface areas for the aqueous explicit-solvent

DOI: 10.1021/acs.jpcb.8b11818
J. Phys. Chem. B 2019, 123, 2756−2769

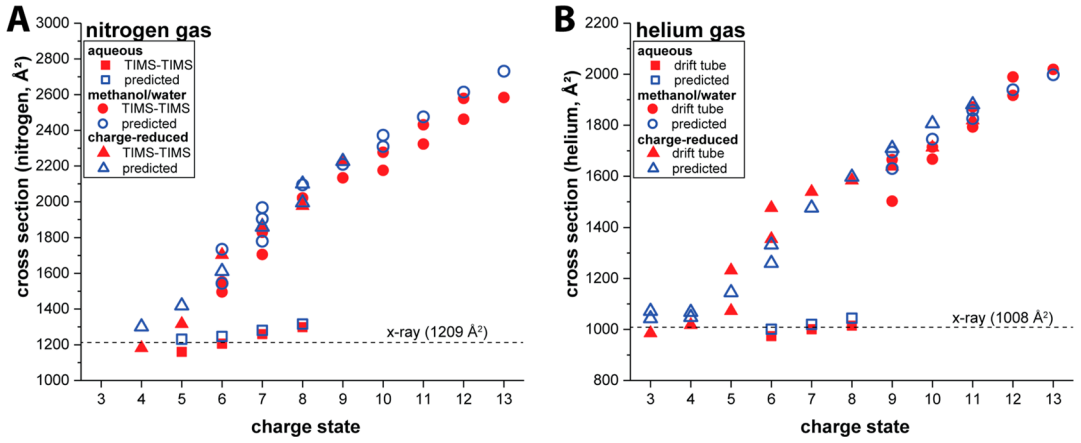

Figure 4. Cross sections of the main features observed in the experimental and SRA-predicted spectra of ubiquitin as a function of the charge state for (A) nitrogen and (B) helium gas. The nitrogen and helium cross sections for the X-ray structure (1UBQ) are indicated (dashed lines). The SRA method accurately predicts the trends observed in the experiments regardless of charge state or experimental condition. The SRA predicts ions produced from aqueous conditions (blue, open squares) to be significantly more compact than their isomers produced from refolding after charge reduction in the gas phase (blue, open triangles) in agreement with the experiment (red, filled squares and triangles, respectively). (Helium experiments taken from refs 31 and 35.)

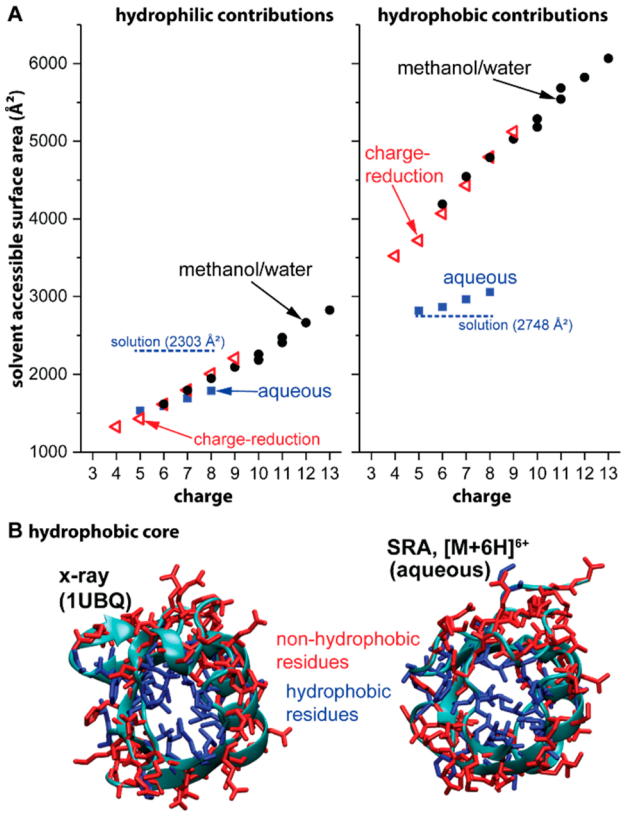

Figure 5. (A) Mean hydrophobic and hydrophilic solvent accessible surface areas predicted by the SRA method for various charge states and experimental conditions of ubiquitin. Dashed lines denote averages calculated for the aqueous explicit-solvent simulations. Gas-phase relaxation decreases the hydrophilic surface area of ubiquitin ions produced from aqueous solutions by ~20−30% whereas the hydrophobic surface area increases only by ~2−10%. (B) The SRA method predicts that ubiquitin ions observed from aqueous solution retain their native topology of a hydrophobic core with hydrophilic residues exposed on the protein surface.

simulations (2748 and 2303 Å^2, respectively). The SRA predicts that the gas-phase relaxation decreases the hydrophilic surface area of ubiquitin ions produced from aqueous solutions by ~20−30%. But our data also suggest that ions with the same charge state expose essentially the same hydrophilic surface area to the environment, regardless of whether they are formed from aqueous solution, acidic methanol/water, or refolded in the gas phase after proton abstraction. By contrast, the hydrophobic surface area of charge states 5+ to 8+ produced from aqueous solution is significantly smaller than the hydrophobic surface area of ions formed in a hydrophobic environment (methanol/water or charge reduction in the gas phase). Note also the only minor increase in hydrophobic surface area for the compact features produced from aqueous solvent conditions (~2−10%). This minor increase of the hydrophobic surface area is inconsistent with formation of inside-out ubiquitin structures. Indeed, the SRA predicts that ubiquitin ions formed from an aqueous solution largely retain their native topology of a hydrophobic core with hydrophilic residues exposed on the surface (Figure 5B).

How can, at least on the time scale of "soft" ion mobility measurements, ubiquitin ions retain their native topology with a hydrophobic core and hydrophilic residues exposed to the hydrophobic gas phase?

At first glance, being apolar, the gas phase might appear to be a hydrophobic environment similar to that of a biological membrane. This view might suggest that attractive forces between hydrophobic moieties of a protein, such as those within the hydrophobic core of ubiquitin, would be lost in the gas phase,[28−30] rendering the native structure unstable in the gas phase. The hydrophobic force, however, does not truly arise from attractive intermolecular forces between hydrophobic moieties. Rather, hydrophobic "bonding" is only an effective force arising from a complex interplay of solute−solute and solute−protein interactions, as well as intermolecular forces between the hydrophobic moieties.[25] After solvent evaporation, only the intermolecular forces between apolar moieties remain. In general, these intermolecular forces arise from interactions between electronic states of the interacting moieties and are broadly classified as exchange, induction, dispersion, and electrostatic interactions.[91] Symmetry adapted perturbation theory now tells us that intermolecular interactions between apolar moieties arise mainly from dispersion and induction

DOI: 10.1021/acs.jpcb.8b11818
J. Phys. Chem. B 2019, 123, 2756−2769

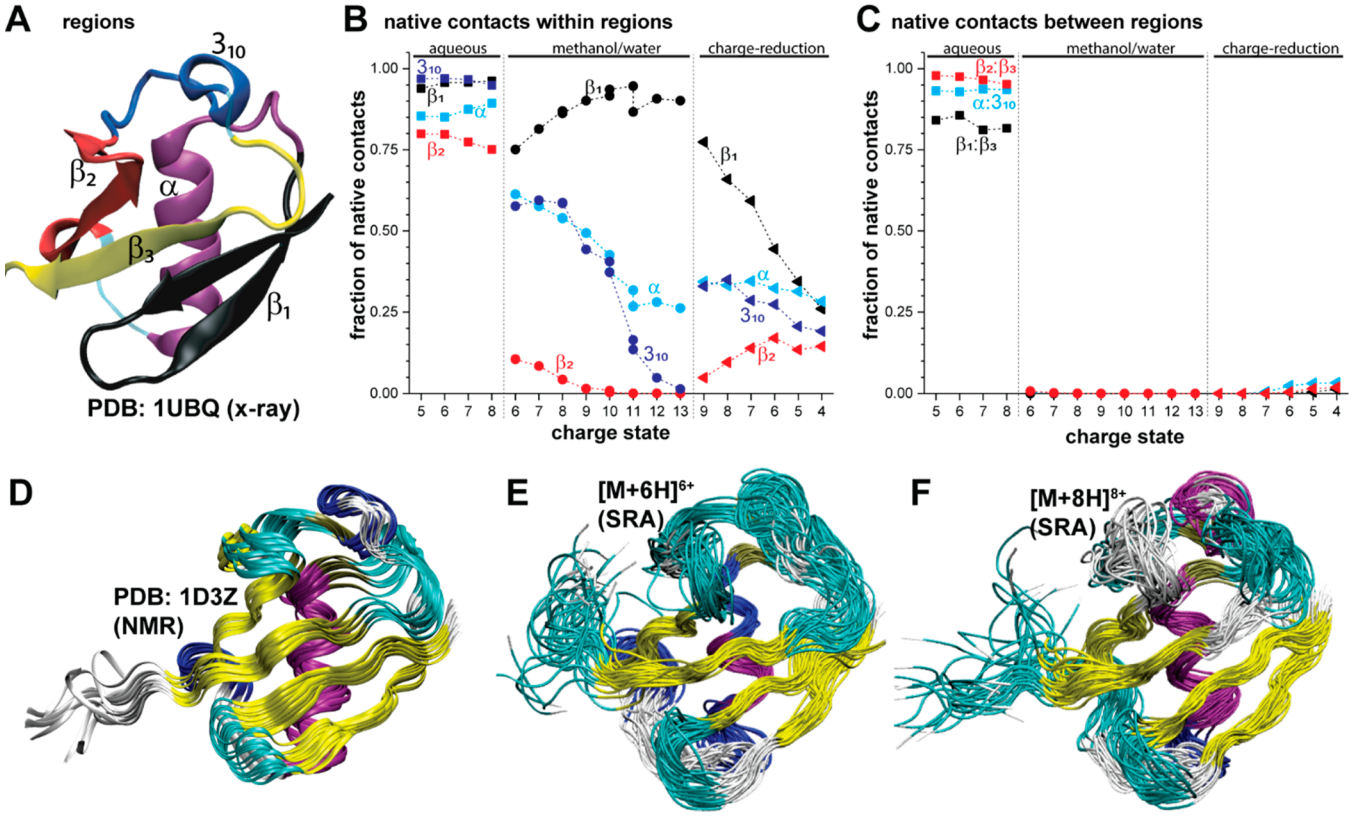

Figure 6. (A) X-ray structure of ubiquitin (1UBQ) with secondary-structure regions indicated (β_1, α, β_2, 3_{10}, β_3). Fraction of native contacts predicted by the SRA method for various charge states and experimental conditions (B) within each region and (C) between the regions. Note that β_3 lacks contacts in the native (X-ray) structure. Inter-residue contacts of ions produced from aqueous solution are highly similar to those in the X-ray structure ($Q > 0.75$ for all regions), indicating that ubiquitin ions detected in these ion mobility experiments strongly resemble the X-ray structure. (D) Ensemble of solution NMR structures for ubiquitin (1D3Z) with secondary structure indicated by STRIDE (β-strand, yellow; α-helix, purple; 3_{10}-helix, blue; turn, cyan). (E), (F) Ensemble of structures predicted by the SRA for $[M + 6H]^{6+}$ and $[M + 8H]^{8+}$, respectively, from aqueous conditions. These ions are predicted to retain the overall topology and most of the secondary structure of the native structure. The same conclusions also follow from SRA predictions for helium buffer gas.

interactions.[92,93] Because dispersive and inductive interactions are always attractive in nature, the environment of the protein (solution or gas phase) should bear little influence of the intrinsic stability of a hydrophobic core. Furthermore, exposing (even parts of) a hydrophobic core to the environment requires reorganization of the protein backbone, and thus higher energy barriers to be overcome. By contrast, hydrophilic patches are readily removed from the surface of a protein by internal rotations of the amino acid side chains.[30,75,76,94] These considerations suggest that exposing hydrophobic patches on a protein surface is unlikely the driving force for the isomerization of protein systems after solvent evaporation.

How Closely Does the Structure of Ubiquitin Ions Detected by Ion Mobility Resemble Their Native Structure? A more detailed picture of ubiquitin structures detected in the ion mobility measurements emerges from analyzing the fraction of native contacts with respect to the X-ray structure. The fraction of native contacts Q is a widely used measure to characterize protein conformations during protein folding.[95,96] The values of Q vary between 0.0 and 1.0, where a value close to 1.0 means that the particular region is governed by the same inter-residue contacts as X-ray structure (and vice versa).

The native state of ubiquitin[90] involves a high content of secondary-structure elements, including a five-stranded β-sheet from three different sequence regions, an α-helix (fitting into a concavity formed by the β-sheet), and a 3_{10}-helix (Figure 6A). To more specifically identify which aspects of the ubiquitin structure change most strongly after solvent evaporation, we calculate the fraction of native contacts with respect to the X-ray structure separately for the five different regions of ubiquitin (α, 3_{10}, β_1, β_2, β_3).

We plot the fraction of native contacts Q predicted by the SRA *within* these regions in Figure 6B for the various charge states, whereas Figure 6C plots the fraction of native contacts *between* the different regions. The data show that the inter-residue contacts of ions produced from aqueous solution are highly similar to those in the X-ray structure ($Q > 0.75$) for all regions. Note that this agreement applies to all inter-residue contacts, i.e., within the various regions (Figure 6B), as well as to the contacts between the regions (Figure 6C). Our analysis thus indicates that the structures of the ubiquitin ions detected in these ion mobility experiments strongly resemble the X-ray structure. Figure S11 (Supporting Information) indicates that the same conclusion follows from analysis of the helium spectra predicted by the SRA method for data recorded on a drift tube by Wyttenbach et al.[31] We compare the structural ensemble recorded by solution NMR spectroscopy to the SRA ensembles for ubiquitin $[M + 6H]^{6+}$ and $[M + 8H]^{8+}$ in Figure 6D–F. The figures illustrate that the SRA ensembles predicted for $[M + 6H]^{6+}$ and $[M + 8H]^{8+}$ strongly resemble the topology of the ubiquitin NMR structure. This prediction is supported by prior theoretical studies on ubiquitin.[43,74]

DOI: 10.1021/acs.jpcb.8b11818
J. Phys. Chem. B 2019, 123, 2756–2769

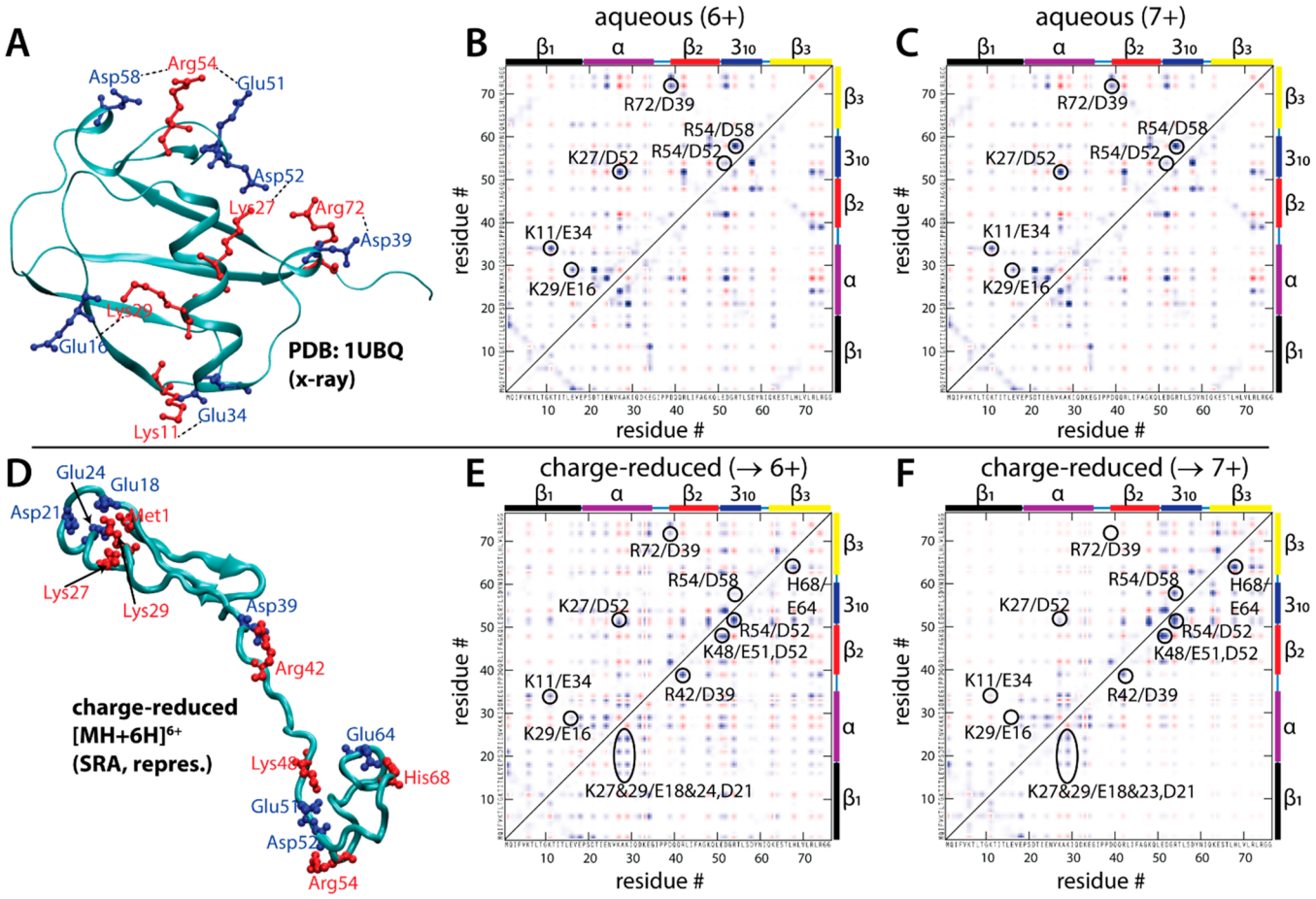

Figure 7. (A) X-ray structure of ubiquitin (1UBQ) with stabilizing salt-bridges indicated. (B), (C) Residue−residue interaction maps predicted by the SRA at the PM6 level of theory for $[M + 6H]^{6+}$ and $[M + 7H]^{7+}$ ions from aqueous conditions. The SRA predicts that salt bridges that stabilize the ubiquitin native structure also stabilize $[M + 6H]^{6+}$ and $[M + 7H]^{7+}$. (D) Representative structure (SRA) for refolded, charge-reduced $[M + 6H]^{6+}$ with important salt bridges indicated. (E), (F) Residue−residue interaction maps predicted by the SRA for $[M + 6H]^{6+}$ and $[M + 7H]^{7+}$ after charge reduction and refolding in the gas phase. Native salt bridges are considerably weakened and replaced by interactions between proximate residues as illustrated in (D).

Ions produced from acidic methanol/water exhibit strongly native inter-residue contacts within the β_1-region (Figure 6B). We make the same observation for the two helical regions, albeit the inter-residue contacts in these regions deviate increasingly from the X-ray structure with increasing charge state. Inter-residue contacts in the β_2-region resembling the X-ray structure are not found. Note that contacts between the various regions differ from the X-ray structure (Figure 6C). We note that the ubiquitin A-state prevalent in acidic methanol/water resembles the X-ray structures within the β_1 and the two helical regions, but not in the β_2-region or between the regions.[72] This presence of a β-sheet in the N-terminal region of ubiquitin was previously reported in a coupled ion mobility/ultraviolet photodissociation study for charge state 11+ produced from an acidic methanol/water solution.[97] We note, however, that this N-terminal β-sheet is not present in high-energy conformations[58] and the putative global minimum[98] of charge state 13+, which points to the significance of accounting in the modeling for the lack of ergodicity of "soft" ion mobility experiments.

For the charge-reduced ubiquitin species, Figure 6B reveals that the β_1-region resembles somewhat the native structure and the A-state but all other regions are strongly non-native. We further cannot identify native inter-residue contacts between the regions in any of the charge-reduced species (Figure 6C). These observations thus indicate that the charge-reduced species differ from their isomers generated from aqueous solution as well as those from acidic methanol/water. We emphasize this because cross sections of several charge-reduced species agree well with cross sections of the isomers produced from methanol/water solutions (Figure 4). This observation further underscores that agreement in cross section does not imply similarity in structures.

Are Native Salt-Bridges Retained upon Solvent Evaporation? The ubiquitin native state[90] stabilizes the arrangement of the various secondary-structure elements by several salt bridges (Figure 7A), most notably by interactions between Lys11/Glu34 and Lys27/Asp52 anchoring the α-helix to the five-stranded β-sheet.

Parts B and C of Figure 7 show residue−residue interaction maps predicted by the SRA at the PM6 level of theory[99] for the dominant peaks of $[M + 6H]^{6+}$ and $[M + 7H]^{7+}$ ions, respectively, generated from aqueous conditions. Such maps reveal how strongly two residues interact with each other (see section S2.3.8, Supporting Information, for details). The data indicate that the salt bridges that stabilize the ubiquitin native state (Figure 7A) also stabilize the $[M + 6H]^{6+}$ (Figure 7B) and $[M + 7H]^{7+}$ (Figure 7C). In particular, the salt-bridges between Lys11/Glu34 (3.2 and 2.6 kcal/mol, respectively, for charge

DOI: 10.1021/acs.jpcb.8b11818
J. Phys. Chem. B 2019, 123, 2756−2769

state 6+ and 7+) and Lys27/Asp52 (4.0 kcal/mol for charge state 6+ and 7+) remain strongly bonding, tethering the α-helix to the five-stranded β-sheet. Figure 7D shows a representative snapshot from the SRA predictions for charge-reduced, refolded $[M + 6H]^{6+}$ while Figure 7E,F plot the interaction maps for the charge-reduced $[M + 6H]^{6+}$ and $[M + 7H]^{7+}$ species. The plots reveal that the salt bridges that stabilize the ubiquitin native state (Figure 7A) are significantly weakened and replaced by interactions between residues in proximity to each other (i.e., Lys27, Lys29 interacting with Glu18, Asp21, Glu24; see Figure 7D). In particular, the interactions between Lys11/Glu34 and Lys27/Asp52 are reduced to about 1 and 0.5 kcal/mol for the charge-reduced $[M + 6H]^{6+}$ and $[M + 7H]^{7+}$ species, respectively. Overall, Figure 7 indicates that ubiquitin ions detected by ion mobility spectrometry from aqueous conditions are stabilized by the same salt bridges as the ubiquitin native state. By contrast, native salt bridges are replaced in their gas-phase isomers by local interactions between residues close to each other in the polypeptide chain. This process is likely initiated when hydrophilic moieties are charge-solvated[41,75] and removed from the surface of a protein by internal rotations.[75,94] The extended nature of charge-reduced species with remote clusters of charge-solvated residues (Figure 7D), however, is expected to facilitate internal rotations of backbone single bonds. Hence, entropic considerations are likely to contribute to the unfolding of proteins in the gas phase in addition to energetic stabilization through charge-solvation processes.

How Do Ubiquitin Ions Unfold Mechanistically? As discussed,[31,32,37] ubiquitin charge states 6+, 7+, and 8+ from native conditions unfold sequentially from compact into partially unfolded and extended conformations. Figure 8A plots the experimental ion mobility spectrum of ubiquitin charge state 8+ and the spectrum predicted by the SRA (with compact, partially unfolded, and extended regions indicated). According to the SRA, the partially unfolded conformation is formed from the compact conformation when the interaction between the β_1 and β_3 regions (residues 1−18 and 62−76) is disrupted, while the N-terminal β_1 and α-helix regions remain largely in their native fold (Figure 8B). Subsequently, according to the SRA, extended ubiquitin conformations emerge when the interaction between the β_2 and β_3 regions and those of the α- and 3_{10} helices is lost. We probe these predictions by studying the early transitions of the unfolding of charge state 8+ by sequential molecular dynamics simulations at gradually increasing temperatures as described.[58] Figures 8C and S17 (Supporting Information) show that this approach reveals the same unfolding mechanism as predicted by the SRA. Further support for the SRA predictions arises from a study employing microsecond time-scale simulations of ubiquitin charge state 6+.[74] Here, partially unfolded ubiquitin conformations were observed as intermediates that lack interactions between the β_1 and β_3 regions while the N-terminal β_1 and α-helix regions remain largely folded.

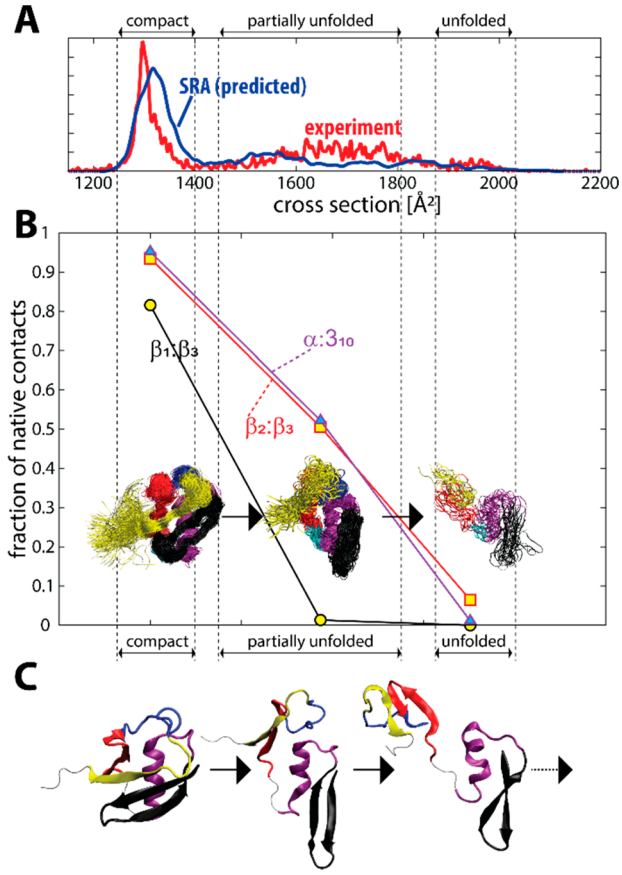

Figure 8. (A) Ion mobility spectrum recorded for ubiquitin charge state 8+ obtained from native conditions to the corresponding spectrum predicted by the SRA. Different regions corresponding to compact, partially unfolded, and extended ubiquitin conformations are indicated. (B) Fraction of native contacts predicted for the compact, partially unfolded, and extended conformations for the interactions between the three β-strand regions and the two helices. (See also Figures 6 and 7.) The SRA predicts that the key step in the unfolding of ubiquitin ions in the gas phase is loss of the interaction between the regions of the first (residues 1−18) and the third β-strand (residues 62−76). (C) Early intermediate states identified from a sequence of molecular dynamics simulations conducted at gradually increasing temperatures support these SRA predictions.

SUMMARY AND CONCLUSIONS

We developed the structure relaxation approximation (SRA) method. The central idea of the SRA is to interpret the trends contained in ion mobility data "globally", thereby allowing detailed structure elucidation. This is enabled by predicting charge-state specific ion mobility spectra from an ensemble of solution structures. The more charge states and experimental conditions are probed by experiment and theory, the greater the confidence of the structural interpretation because chance agreement for all conditions becomes increasingly unlikely. We subsequently applied the SRA to probe how closely, and in which aspects, ions of the protein ubiquitin detected by "soft" ion mobility measurements resemble their native state. To this end, we predicted ion mobility spectra recorded for 34 measurements that differ in charge states, initial (solution) conditions and buffer gases. We find that the SRA method predicts the trends observed in the experiments within the error of the methods.

Specifically, the SRA predicts for the protein ubiquitin:

(1) Ubiquitin ions detected from aqueous conditions by "soft" ion mobility measurements largely retain their hydrophobic core present in their native structure.
(2) Ubiquitin ions detected from aqueous conditions by "soft" ion mobility measurements largely retain their native inter-residue contacts and secondary-structure elements.
(3) If ubiquitin ions are given sufficient energy and time to overcome energy barriers and fold into their gas-phase

DOI: 10.1021/acs.jpcb.8b11818
J. Phys. Chem. B 2019, 123, 2756−2769

structures, native inter-residue contacts are largely replaced by local interactions between proximate residues.

(4) Loss of interaction between the N-terminal and C-terminal β-strand regions is the first step in the unfolding of ubiquitin ions produced from aqueous conditions by "soft" ion mobility measurements.

In sum, the SRA method predicts that, when studied under native conditions by "soft" ion mobility measurements, even proteins as small as ubiquitin largely retain their native structures.

■ ASSOCIATED CONTENT

Supporting Information

The Supporting Information is available free of charge on the ACS Publications website at DOI: 10.1021/acs.jpcb.8b11818.

Full experimental and computational details, pseudocode, flowchart for the method developed, TIMS-TIMS apparatus, isotopic distributions, cross sections for the main features, general structure of the heating protocol used, SRA spectra, $\delta\Omega$ and coherence vs T_{max}, structural dynamics in the gas phase, shape factor analysis, ion mobility spectra, degree of agreement between experimental and predicted spectra, mean solvent accessible surface areas, fraction of native contacts, charge locations, protomers predicted by the SRA method, fraction of native contacts and unfolding pathway, (PDF)

■ AUTHOR INFORMATION

Corresponding Author

*E-mail: cbleiholder@fsu.edu. Phone: +1-850-645-1290.

ORCID

Christian Bleiholder: 0000-0002-4211-1388

Fanny C. Liu: 0000-0003-1403-7114

Author Contributions

The manuscript was written through contributions of all authors.

Funding

CHE-1654608 (National Science Foundation).

Notes

The authors declare no competing financial interest.

The SRA method implementation is available at psa.chem.fsu.edu.

Biography

Christian Bleiholder is an Assistant Professor of Chemistry and Biochemistry at the Florida State University with a M.Sc. and D.Sc. in Chemistry (University of Heidelberg, 2004 & German Cancer Research Center, 2007). Using theoretical methods, he investigated noncovalent self-assembly reactions with Rolf Gleiter and peptide fragmentation used in mass spectrometry-based proteomics methods with Béla Paizs and Sándor Suhai. During his postdoctoral research with Michael T. Bowers (University of California, Santa Barbara) he applied ion mobility/mass spectrometry methods to study formation and inhibition of amyloid fibrils implicated in Alzheimer's Disease. Current research focuses on development of computational and experimental ion mobility spectrometry methods and their application to protein structure and reactivity. His awards include an Alexander-von-Humboldt fellowship (2008–2010), a Postdoctoral Research Award from the American Chemical Society (2011), and a CAREER award from the National Science Foundation (2017).

■ ACKNOWLEDGMENTS

This work was supported by the National Science Foundation under grant CHE-1654608 (C.B.). The authors thank T. Wyttenbach for providing electronic copies of their drift-tube spectra in helium and ubiquitin structures from ref 58.

■ REFERENCES

(1) Robinson, C. V.; Sali, A.; Baumeister, W. The Molecular Sociology of the Cell. *Nature* **2007**, *450*, 973–982.

(2) Clemmer, D. E.; Russell, D. H.; Williams, E. R. Characterizing the *Conformationome*: Toward a Structural Understanding of the Proteome. *Acc. Chem. Res.* **2017**, *50*, 556–560.

(3) Smith, L. M.; Kelleher, N. L. Proteoforms as the next Proteomics Currency. *Science* **2018**, *359*, 1106–1107.

(4) Yang, X.; Coulombe-Huntington, J.; Kang, S.; Sheynkman, G. M.; Hao, T.; Richardson, A.; Sun, S.; Yang, F.; Shen, Y. A.; Murray, R. R.; et al. Widespread Expansion of Protein Interaction Capabilities by Alternative Splicing. *Cell* **2016**, *164*, 805–817.

(5) Kanu, A. B.; Dwivedi, P.; Tam, M.; Matz, L.; Hill, H. H. Ion Mobility-Mass Spectrometry. *J. Mass Spectrom.* **2008**, *43*, 1–22.

(6) Lanucara, F.; Holman, S. W.; Gray, C. J.; Eyers, C. E. The Power of Ion Mobility-Mass Spectrometry for Structural Characterization and the Study of Conformational Dynamics. *Nat. Chem.* **2014**, *6*, 281–294.

(7) Polasky, D. A.; Lermyte, F.; Nshanian, M.; Sobott, F.; Andrews, P. C.; Loo, J. A.; Ruotolo, B. T. Fixed-Charge Trimethyl Pyrilium Modification for Enabling Enhanced Top-Down Mass Spectrometry Sequencing of Intact Protein Complexes. *Anal. Chem.* **2018**, *90*, 2756–2764.

(8) Zinnel, N. F.; Pai, P.-J.; Russell, D. H. Ion Mobility-Mass Spectrometry (IM-MS) for Top-Down Proteomics: Increased Dynamic Range Affords Increased Sequence Coverage. *Anal. Chem.* **2012**, *84*, 3390–3397.

(9) Greer, S. M.; Brodbelt, J. S. Top-Down Characterization of Heavily Modified Histones Using 193 Nm Ultraviolet Photodissociation Mass Spectrometry. *J. Proteome Res.* **2018**, *17*, 1138–1145.

(10) Cleland, T. P.; DeHart, C. J.; Fellers, R. T.; VanNispen, A. J.; Greer, J. B.; LeDuc, R. D.; Parker, W. R.; Thomas, P. M.; Kelleher, N. L.; Brodbelt, J. S. High-Throughput Analysis of Intact Human Proteins Using UVPD and HCD on an Orbitrap Mass Spectrometer. *J. Proteome Res.* **2017**, *16*, 2072–2079.

(11) Shelimov, K. B.; Clemmer, D. E.; Hudgins, R. R.; Jarrold, M. F. Protein Structure *in Vacuo*: Gas-Phase Conformations of BPTI and Cytochrome *C*. *J. Am. Chem. Soc.* **1997**, *119*, 2240–2248.

(12) Bleiholder, C.; Dupuis, N. F.; Wyttenbach, T.; Bowers, M. T. Ion Mobility–Mass Spectrometry Reveals a Conformational Conversion from Random Assembly to β-Sheet in Amyloid Fibril Formation. *Nat. Chem.* **2011**, *3*, 172–177.

(13) Bleiholder, C.; Do, T. D.; Wu, C.; Economou, N. J.; Bernstein, S. S.; Buratto, S. K.; Shea, J.-E.; Bowers, M. T. Ion Mobility Spectrometry Reveals the Mechanism of Amyloid Formation of Aβ(25–35) and Its

DOI: 10.1021/acs.jpcb.8b11818
J. Phys. Chem. B 2019, 123, 2756–2769

Modulation by Inhibitors at the Molecular Level: Epigallocatechin Gallate and *Scyllo* -Inositol. *J. Am. Chem. Soc.* **2013**, *135*, 16926−16937.
(14) Mao, Y.; Woenckhaus, J.; Kolafa, J.; Ratner, M. A.; Jarrold, M. F. Thermal Unfolding of Unsolvated Cytochrome *c*: Experiment and Molecular Dynamics Simulations. *J. Am. Chem. Soc.* **1999**, *121*, 2712−2721.
(15) Zhong, Y.; Han, L.; Ruotolo, B. T. Collisional and Coulombic Unfolding of Gas-Phase Proteins: High Correlation to Their Domain Structures in Solution. *Angew. Chem., Int. Ed.* **2014**, *53*, 9209−9212.
(16) Shi, H.; Atlasevich, N.; Merenbloom, S. I.; Clemmer, D. E. Solution Dependence of the Collisional Activation of Ubiquitin [M + 7H]7+ Ions. *J. Am. Soc. Mass Spectrom.* **2014**, *25*, 2000−2008.
(17) Clemmer, D. E.; Jarrold, M. F. Ion Mobility Measurements and Their Applications to Clusters and Biomolecules. *J. Mass Spectrom.* **1997**, *32*, 577−592.
(18) Konijnenberg, A.; Bannwarth, L.; Yilmaz, D.; Koçer, A.; Venien-Bryan, C.; Sobott, F. Top-down Mass Spectrometry of Intact Membrane Protein Complexes Reveals Oligomeric State and Sequence Information in a Single Experiment: Top-down MS of Membrane Proteins. *Protein Sci.* **2015**, *24*, 1292−1300.
(19) Koeniger, S. L.; Merenbloom, S. I.; Valentine, S. J.; Jarrold, M. F.; Udseth, H. R.; Smith, R. D.; Clemmer, D. E. An IMS−IMS Analogue of MS−MS. *Anal. Chem.* **2006**, *78*, 4161−4174.
(20) Liu, F. C.; Ridgeway, M. E.; Park, M. A.; Bleiholder, C. Tandem Trapped Ion Mobility Spectrometry. *Analyst* **2018**, *143*, 2249−2258.
(21) Revercomb, H. E.; Mason, E. A. Theory of Plasma Chromatography/Gaseous Electrophoresis. Review. *Anal. Chem.* **1975**, *47*, 970−983.
(22) Mason, E. A.; McDaniel, E. W. *Transport Properties of Ions in Gases*; Wiley-VCH: Weinheim, Germany, 1988.
(23) Bleiholder, C. Towards Measuring Ion Mobilities in Non-Stationary Gases and Non-Uniform and Dynamic Electric Fields (I). Transport Equation. *Int. J. Mass Spectrom.* **2016**, *399*−*400*, 1−9.
(24) Gruebele, M. Protein Folding: The Free Energy Surface. *Curr. Opin. Struct. Biol.* **2002**, *12*, 161−168.
(25) Bellissent-Funel, M.-C.; Hassanali, A.; Havenith, M.; Henchman, R.; Pohl, P.; Sterpone, F.; van der Spoel, D.; Xu, Y.; Garcia, A. E. Water Determines the Structure and Dynamics of Proteins. *Chem. Rev.* **2016**, *116*, 7673−7697.
(26) Wolynes, P. G. Biomolecular Folding in Vacuo!!!(?). *Proc. Natl. Acad. Sci. U. S. A.* **1995**, *92*, 2426−2427.
(27) Meyer, T.; Gabelica, V.; Grubmüller, H.; Orozco, M. Proteins in the Gas Phase: Proteins in the Gas Phase. *Wiley Interdiscip. Rev. Comput. Mol. Sci.* **2013**, *3*, 408−425.
(28) Breuker, K.; Oh, H.; Horn, D. M.; Cerda, B. A.; McLafferty, F. W. Detailed Unfolding and Folding of Gaseous Ubiquitin Ions Characterized by Electron Capture Dissociation. *J. Am. Chem. Soc.* **2002**, *124*, 6407−6420.
(29) Skinner, O. S.; McLafferty, F. W.; Breuker, K. How Ubiquitin Unfolds after Transfer into the Gas Phase. *J. Am. Soc. Mass Spectrom.* **2012**, *23*, 1011−1014.
(30) Breuker, K.; McLafferty, F. W. Stepwise Evolution of Protein Native Structure with Electrospray into the Gas Phase, 10^{-12} to 10^{2} S. *Proc. Natl. Acad. Sci. U. S. A.* **2008**, *105*, 18145−18152.
(31) Wyttenbach, T.; Bowers, M. T. Structural Stability from Solution to the Gas Phase: Native Solution Structure of Ubiquitin Survives Analysis in a Solvent-Free Ion Mobility−Mass Spectrometry Environment. *J. Phys. Chem. B* **2011**, *115*, 12266−12275.
(32) Myung, S.; Badman, E. R.; Lee, Y. J.; Clemmer, D. E. Structural Transitions of Electrosprayed Ubiquitin Ions Stored in an Ion Trap over ∼ 10 Ms to 30 S. *J. Phys. Chem. A* **2002**, *106*, 9976−9982.
(33) Allen, S. J.; Eaton, R. M.; Bush, M. F. Structural Dynamics of Native-Like Ions in the Gas Phase: Results from Tandem Ion Mobility of Cytochrome *C*. *Anal. Chem.* **2017**, *89*, 7527−7534.
(34) El-Baba, T. J.; Woodall, D. W.; Raab, S. A.; Fuller, D. R.; Laganowsky, A.; Russell, D. H.; Clemmer, D. E. Melting Proteins: Evidence for Multiple Stable Structures upon Thermal Denaturation of Native Ubiquitin from Ion Mobility Spectrometry-Mass Spectrometry Measurements. *J. Am. Chem. Soc.* **2017**, *139*, 6306−6309.
(35) Laszlo, K. J.; Munger, E. B.; Bush, M. F. Folding of Protein Ions in the Gas Phase after Cation-to-Anion Proton-Transfer Reactions. *J. Am. Chem. Soc.* **2016**, *138*, 9581−9588.
(36) Jhingree, J. R.; Beveridge, R.; Dickinson, E. R.; Williams, J. P.; Brown, J. M.; Bellina, B.; Barran, P. E. Electron Transfer with No Dissociation Ion Mobility−Mass Spectrometry (ETnoD IM-MS). The Effect of Charge Reduction on Protein Conformation. *Int. J. Mass Spectrom.* **2017**, *413*, 43−51.
(37) Koeniger, S. L.; Merenbloom, S. I.; Sevugarajan, S.; Clemmer, D. E. Transfer of Structural Elements from Compact to Extended States in Unsolvated Ubiquitin. *J. Am. Chem. Soc.* **2006**, *128*, 11713−11719.
(38) von Helden, G.; Hsu, M. T.; Gotts, N.; Bowers, M. T. Carbon Cluster Cations with up to 84 Atoms: Structures, Formation Mechanism, and Reactivity. *J. Phys. Chem.* **1993**, *97*, 8182−8192.
(39) Shvartsburg, A. A.; Liu, B.; Jarrold, M. F.; Ho, K.-M. Modeling Ionic Mobilities by Scattering on Electronic Density Isosurfaces: Application to Silicon Cluster Anions. *J. Chem. Phys.* **2000**, *112*, 4517−4526.
(40) von Helden, G.; Wyttenbach, T.; Bowers, M. T. Inclusion of a MALDI Ion Source in the Ion Chromatography Technique: Conformational Information on Polymer and Biomolecular Ions. *Int. J. Mass Spectrom. Ion Processes* **1995**, *146*, 349−364.
(41) Wyttenbach, T.; von Helden, G.; Bowers, M. T. Gas-Phase Conformation of Biological Molecules: Bradykinin. *J. Am. Chem. Soc.* **1996**, *118*, 8355−8364.
(42) Jurneczko, E.; Barran, P. E. How Useful Is Ion Mobility Mass Spectrometry for Structural Biology? The Relationship between Protein Crystal Structures and Their Collision Cross Sections in the Gas Phase. *Analyst* **2011**, *136*, 20−28.
(43) Chen, S.-H.; Russell, D. H. How Closely Related Are Conformations of Protein Ions Sampled by IM-MS to Native Solution Structures? *J. Am. Soc. Mass Spectrom.* **2015**, *26*, 1433−1443.
(44) Johnson, R. E. Atomic and Molecular Collisions. *Encyclopedia of Physical Science and Technology*; Academic Press, 1987; Vol. *2*, pp 224−251.
(45) Levinthal, C. How to Fold Graciously. *Proceedings of a meeting held at Allerton House*; University of Illinois Press: Monticello, IL, 1969; pp 22−24.
(46) Bowers, M. T.; Kemper, P. R.; Helden, G. von; Koppen, P. A. M. van. Gas-Phase Ion Chromatography: Transition Metal State Selection and Carbon Cluster Formation. *Science* **1993**, *260*, 1446−1451.
(47) Bleiholder, C.; Bowers, M. T. The Solution Assembly of Biological Molecules Using Ion Mobility Methods: From Amino Acids to Amyloid *β*-Protein. *Annu. Rev. Anal. Chem.* **2017**, *10*, 365−386.
(48) Seo, J.; Hoffmann, W.; Warnke, S.; Huang, X.; Gewinner, S.; Schöllkopf, W.; Bowers, M. T.; von Helden, G.; Pagel, K. An Infrared Spectroscopy Approach to Follow *β*-Sheet Formation in Peptide Amyloid Assemblies. *Nat. Chem.* **2017**, *9*, 39−44.
(49) Ibarra-Molero, B.; Loladze, V. V.; Makhatadze, G. I.; Sanchez-Ruiz, J. M. Thermal versus Guanidine-Induced Unfolding of Ubiquitin. An Analysis in Terms of the Contributions from Charge−Charge Interactions to Protein Stability. *Biochemistry* **1999**, *38*, 8138−8149.
(50) Liu, F. C.; Kirk, S. R.; Bleiholder, C. On the Structural Denaturation of Biological Analytes in Trapped Ion Mobility Spectrometry − Mass Spectrometry. *Analyst* **2016**, *141*, 3722−3730.
(51) Bleiholder, C.; Johnson, N. R.; Contreras, S.; Wyttenbach, T.; Bowers, M. T. Molecular Structures and Ion Mobility Cross Sections: Analysis of the Effects of He and N_2 Buffer Gas. *Anal. Chem.* **2015**, *87*, 7196−7203.
(52) May, J. C.; Jurneczko, E.; Stow, S. M.; Kratochvil, I.; Kalkhof, S.; McLean, J. A. Conformational Landscapes of Ubiquitin, Cytochrome c, and Myoglobin: Uniform Field Ion Mobility Measurements in Helium and Nitrogen Drift Gas. *Int. J. Mass Spectrom.* **2018**, *427*, 79.
(53) Silveira, J. A.; Ridgeway, M. E.; Park, M. A. High Resolution Trapped Ion Mobility Spectrometery of Peptides. *Anal. Chem.* **2014**, *86*, 5624−5627.
(54) Michelmann, K.; Silveira, J. A.; Ridgeway, M. E.; Park, M. A. Fundamentals of Trapped Ion Mobility Spectrometry. *J. Am. Soc. Mass Spectrom.* **2015**, *26*, 14−24.

DOI: 10.1021/acs.jpcb.8b11818
J. Phys. Chem. B 2019, 123, 2756−2769

(55) Hernandez, D. R.; DeBord, J. D.; Ridgeway, M. E.; Kaplan, D. A.; Park, M. A.; Fernandez-Lima, F. Ion Dynamics in a Trapped Ion Mobility Spectrometer. *Analyst* **2014**, *139*, 1913−1921.
(56) Chai, M.; Young, M. N.; Liu, F. C.; Bleiholder, C. A. Transferable, Sample-Independent Calibration Procedure for Trapped Ion Mobility Spectrometry (TIMS). *Anal. Chem.* **2018**, *90*, 9040−9047.
(57) Stow, S. M.; Causon, T. J.; Zheng, X.; Kurulugama, R. T.; Mairinger, T.; May, J. C.; Rennie, E. E.; Baker, E. S.; Smith, R. D.; McLean, J. A.; et al. An Interlaboratory Evaluation of Drift Tube Ion Mobility−Mass Spectrometry Collision Cross Section Measurements. *Anal. Chem.* **2017**, *89*, 9048−9055.
(58) Segev, E.; Wyttenbach, T.; Bowers, M. T.; Gerber, R. B. Conformational Evolution of Ubiquitin Ions in Electrospray Mass Spectrometry: Molecular Dynamics Simulations at Gradually Increasing Temperatures. *Phys. Chem. Chem. Phys.* **2008**, *10*, 3077−3082.
(59) Berendsen, H. J. C.; van der Spoel, D.; van Drunen, R. GROMACS: A Message-Passing Parallel Molecular Dynamics Implementation. *Comput. Phys. Commun.* **1995**, *91*, 43−56.
(60) Duan, Y.; Wu, C.; Chowdhury, S.; Lee, M. C.; Xiong, G.; Zhang, W.; Yang, R.; Cieplak, P.; Luo, R.; Lee, T.; et al. A Point-Charge Force Field for Molecular Mechanics Simulations of Proteins Based on Condensed-Phase Quantum Mechanical Calculations. *J. Comput. Chem.* **2003**, *24*, 1999−2012.
(61) Jorgensen, W. L.; Chandrasekhar, J.; Madura, J. D.; Impey, R. W.; Klein, M. L. Comparison of Simple Potential Functions for Simulating Liquid Water. *J. Chem. Phys.* **1983**, *79*, 926−935.
(62) Wang, J.; Cieplak, P.; Kollman, P. A. How Well Does a Restrained Electrostatic Potential (RESP) Model Perform in Calculating Conformational Energies of Organic and Biological Molecules? *J. Comput. Chem.* **2000**, *21*, 1049−1074.
(63) Jorgensen, W. L.; Tirado-Rives, J. The OPLS Potential Functions for Proteins. Energy Minimizations for Crystals of Cyclic Peptides and Crambin. *J. Am. Chem. Soc.* **1988**, *110*, 1657−1666.
(64) Kaminski, G. A.; Friesner, R. A.; Tirado-Rives, J.; Jorgensen, W. L. Evaluation and Reparametrization of the OPLS-AA Force Field for Proteins via Comparison with Accurate Quantum Chemical Calculations on Peptides. *J. Phys. Chem. B* **2001**, *105*, 6474−6487.
(65) Kaminski, G. A.; Stern, H. A.; Berne, B. J.; Friesner, R. A.; Cao, Y. X.; Murphy, R. B.; Zhou, R.; Halgren, T. A. Development of a Polarizable Force Field for Proteins via Ab Initio Quantum Chemistry: First Generation Model and Gas Phase Tests. *J. Comput. Chem.* **2002**, *23*, 1515−1531.
(66) Bleiholder, C.; Wyttenbach, T.; Bowers, M. T. A Novel Projection Approximation Algorithm for the Fast and Accurate Computation of Molecular Collision Cross Sections (I). Method. *Int. J. Mass Spectrom.* **2011**, *308*, 1−10.
(67) Anderson, S. E.; Bleiholder, C.; Brocker, E. R.; Stang, P. J.; Bowers, M. T. A Novel Projection Approximation Algorithm for the Fast and Accurate Computation of Molecular Collision Cross Sections (III): Application to Supramolecular Coordination-Driven Assemblies with Complex Shapes. *Int. J. Mass Spectrom.* **2012**, *330*−*332*, 78−84.
(68) Bleiholder, C.; Contreras, S.; Do, T. D.; Bowers, M. T. A Novel Projection Approximation Algorithm for the Fast and Accurate Computation of Molecular Collision Cross Sections (II). Model Parameterization and Definition of Empirical Shape Factors for Proteins. *Int. J. Mass Spectrom.* **2013**, *345*−*347*, 89−96.
(69) Bleiholder, C.; Contreras, S.; Bowers, M. T. A Novel Projection Approximation Algorithm for the Fast and Accurate Computation of Molecular Collision Cross Sections (IV). Application to Polypeptides. *Int. J. Mass Spectrom.* **2013**, *354*−*355*, 275−280.
(70) Fraternali, F. Parameter Optimized Surfaces (POPS): Analysis of Key Interactions and Conformational Changes in the Ribosome. *Nucleic Acids Res.* **2002**, *30*, 2950−2960.
(71) Stewart, J. J. P. *MOPAC2016*; Stewart Computational Chemistry: Colorado Springs, CO, 2016.
(72) Brutscher, B.; Bruschweiler, R.; Ernst, R. R. Backbone Dynamics and Structural Characterization of the Partially Folded A State of Ubiquitin by 1H, 13C, and 15N Nuclear Magnetic Resonance Spectroscopy. *Biochemistry* **1997**, *36*, 13043−13053.
(73) McAllister, R. G.; Metwally, H.; Sun, Y.; Konermann, L. Release of Native-like Gaseous Proteins from Electrospray Droplets via the Charged Residue Mechanism: Insights from Molecular Dynamics Simulations. *J. Am. Chem. Soc.* **2015**, *137*, 12667−12676.
(74) Bakhtiari, M.; Konermann, L. Protein Ions Generated by Native Electrospray Ionization: Comparison of Gas Phase, Solution, and Crystal Structures. *J. Phys. Chem. B* **2019**, *123*, 1784.
(75) Steinberg, M. Z.; Elber, R.; McLafferty, F. W.; Gerber, R. B.; Breuker, K. Early Structural Evolution of Native Cytochrome c after Solvent Removal. *ChemBioChem* **2008**, *9*, 2417−2423.
(76) Jarrold, M. F. Unfolding, Refolding, and Hydration of Proteins in the Gas Phase. *Acc. Chem. Res.* **1999**, *32*, 360−367.
(77) Kaltashov, I.; Abzalimov, R. Do Ionic Charges in ESI MS Provide Useful Information on Macromolecular Structure? *J. Am. Soc. Mass Spectrom.* **2008**, *19*, 1239−1246.
(78) Stewart, J. J. P. Application of Localized Molecular Orbitals to the Solution of Semiempirical Self-Consistent Field Equations. *Int. J. Quantum Chem.* **1996**, *58*, 133−146.
(79) Konermann, L. Molecular Dynamics Simulations on Gas-Phase Proteins with Mobile Protons: Inclusion of All-Atom Charge Solvation. *J. Phys. Chem. B* **2017**, *121*, 8102−8112.
(80) Sugita, Y.; Okamoto, Y. Replica-Exchange Molecular Dynamics Method for Protein Folding. *Chem. Phys. Lett.* **1999**, *314*, 141−151.
(81) Grubmüller, H. Predicting Slow Structural Transitions in Macromolecular Systems: Conformational Flooding. *Phys. Rev. E: Stat. Phys., Plasmas, Fluids, Relat. Interdiscip. Top.* **1995**, *52*, 2893−2906.
(82) Laio, A.; Parrinello, M. Escaping Free-Energy Minima. *Proc. Natl. Acad. Sci. U. S. A.* **2002**, *99*, 12562−12566.
(83) Mesleh, M. F.; Hunter, J. M.; Shvartsburg, A. A.; Schatz, G. C.; Jarrold, M. F. Structural Information from Ion Mobility Measurements: Effects of the Long-Range Potential. *J. Phys. Chem.* **1996**, *100*, 16082−16086.
(84) Shvartsburg, A. A.; Mashkevich, S. V.; Baker, E. S.; Smith, R. D. Optimization of Algorithms for Ion Mobility Calculations. *J. Phys. Chem. A* **2007**, *111*, 2002−2010.
(85) Alexeev, Y.; Fedorov, D. G.; Shvartsburg, A. A. Effective Ion Mobility Calculations for Macromolecules by Scattering on Electron Clouds. *J. Phys. Chem. A* **2014**, *118*, 6763−6772.
(86) Voronina, L.; Masson, A.; Kamrath, M.; Schubert, F.; Clemmer, D.; Baldauf, C.; Rizzo, T. Conformations of Prolyl−Peptide Bonds in the Bradykinin 1−5 Fragment in Solution and in the Gas Phase. *J. Am. Chem. Soc.* **2016**, *138*, 9224−9233.
(87) Marklund, E. G.; Degiacomi, M. T.; Robinson, C. V.; Baldwin, A. J.; Benesch, J. L. P. Collision Cross Sections for Structural Proteomics. *Structure* **2015**, *23*, 791−799.
(88) Bleiholder, C. A Local Collision Probability Approximation for Predicting Momentum Transfer Cross Sections. *Analyst* **2015**, *140*, 6804−6813.
(89) Young, M. N.; Bleiholder, C. Molecular Structures and Momentum Transfer Cross Sections: The Influence of the Analyte Charge Distribution. *J. Am. Soc. Mass Spectrom.* **2017**, *28*, 619−627.
(90) Vijay-Kumar, S.; Bugg, C. E.; Wilkinson, K. D.; Cook, W. J. Three-Dimensional Structure of Ubiquitin at 2.8 A Resolution. *Proc. Natl. Acad. Sci. U. S. A.* **1985**, *82*, 3582−3585.
(91) Jeziorski, B.; Moszynski, R.; Szalewicz, K. Perturbation Theory Approach to Intermolecular Potential Energy Surfaces of van Der Waals Complexes. *Chem. Rev.* **1994**, *94*, 1887−1930.
(92) Bleiholder, C.; Werz, D. B.; Köppel, H.; Gleiter, R. Theoretical Investigations on Chalcogen−Chalcogen Interactions: What Makes These Nonbonded Interactions Bonding? *J. Am. Chem. Soc.* **2006**, *128*, 2666−2674.
(93) Podeszwa, Rafal; Szalewicz, Krzysztof Physical Origins of Interactions in Dimers of Polycyclic Aromatic Hydrocarbons. *Phys. Chem. Chem. Phys.* **2008**, *10*, 2735−2746.
(94) Warnke, S.; von Helden, G.; Pagel, K. Protein Structure in the Gas Phase: The Influence of Side-Chain Microsolvation. *J. Am. Chem. Soc.* **2013**, *135*, 1177−1180.

DOI: 10.1021/acs.jpcb.8b11818
J. Phys. Chem. B 2019, 123, 2756−2769

(95) Best, R. B.; Hummer, G.; Eaton, W. A. Native Contacts Determine Protein Folding Mechanisms in Atomistic Simulations. *Proc. Natl. Acad. Sci. U. S. A.* **2013**, *110*, 17874−17879.
(96) Best, R. B.; Hummer, G. Reaction Coordinates and Rates from Transition Paths. *Proc. Natl. Acad. Sci. U. S. A.* **2005**, *102*, 6732−6737.
(97) Warnke, S.; Baldauf, C.; Bowers, M. T.; Pagel, K.; von Helden, G. Photodissociation of Conformer-Selected Ubiquitin Ions Reveals Site-Specific *Cis*/*Trans* Isomerization of Proline Peptide Bonds. *J. Am. Chem. Soc.* **2014**, *136*, 10308−10314.
(98) Goldstein, M.; Zmiri, L.; Segev, E.; Wyttenbach, T.; Gerber, R. B. An Atomistic Structure of Ubiquitin + 13 Relevant in Mass Spectrometry: Theoretical Prediction and Comparison with Experimental Cross Sections. *Int. J. Mass Spectrom.* **2014**, *367*, 10−15.
(99) Stewart, J. J. P. Optimization of Parameters for Semiempirical Methods V: Modification of NDDO Approximations and Application to 70 Elements. *J. Mol. Model.* **2007**, *13*, 1173−1213.

DOI: 10.1021/acs.jpcb.8b11818
J. Phys. Chem. B 2019, 123, 2756−2769